ELSEVIER

Journal of Materials Processing Technology 189 (2007) 132–137

Journal of Materials Processing Technology

www.elsevier.com/locate/jmatprotec

Nitrogen spray atomization of molten tin metal: Powder morphology characteristics

Renaud Metz [a,*], Céline Machado [a], Mourad Houabes [a], Julien Pansiot [a], Mazen Elkhatib [a], Ramón Puyanē [b], Mehrdad Hassanzadeh [b]

[a] *Laboratoire Commun Lyon1-CNRS-SNPE Hydrazines et Procédés, UMR 5179, UCB Lyon 1, bâtiment Berthollet (731) 3ème étage, 22 avenue Gaston Berger, F-69622 Villeurbanne Cedex, France*

[b] *AREVA, 1340 Rue de Pinville, 34 965 Montpellier Cedex 2, France*

Received 20 March 2006; received in revised form 7 December 2006; accepted 16 January 2007

Abstract

The gas atomization process used for metal powder production has been studied using a low melting point metal: tin. The influence of two experimental atomization parameters (gas flow rate and gas pressure) and the possibility to preview the particle mean diameter with the Lubanska equation are investigated. The ability of spray processing to control and produce well-defined metal powders with both the desired particle size range and shape is discussed.

Keywords: Melt atomization; Tin; Powder

1. Introduction

The atomization process remains a good choice among the different methods of metal powder production due to the versatility, the quality and purity of the obtained powder, the control of its properties and the potential for mass production [1].

The atomization process, as considered, in the present paper, is the starting step in a new production process of oxide ceramic powders. This new route named Direct Oxidation of a Precursory Alloy (DOPA) leads to a ceramic powder by total oxidation of a metallic alloy powder obtained by atomization [2,3]. The oxide powder can then be pressed and sintered to obtain a bulk ceramic. The precursor metal alloys powders need to be accurately controlled in terms of chemical purity, morphology and particle size distribution. The aim of this study was to further the understanding of the atomization process as a basis for subsequent work on DOPA development and optimization.

A number of studies have been performed to relate the powder properties to the process parameters. Several authors have worked on gas atomization and shown the parameters influence on the final powders [4–14]. These works differ ones from the others by the nature of alloys, the atomization process, etc. It is therefore difficult to correlate them. However, the Lubanska equation [15], which is a modification of the Wigg equation [16], is a typical semi-empirical correlation between the process parameters and the mass median particle, commonly used for metal atomization. It takes into account different experimental parameters such as gas and metal flow rates, gas and metal kinematic viscosities, metal stream diameter and the Weber number. The mass median particle diameter as a function of the operating parameters is given by:

$$d_m = d_t K \left[\frac{\nu_m}{\nu_g} \frac{1 + (M/G)}{W_e} \right]^{1/2}$$

$$= d_t K \left[\frac{\nu_m (1 + M/G) \sigma S^2 \rho_g^2}{\nu_g G^2 \rho d_t} \right]^{1/2}$$

where d_m is the mass median particle diameter (m), d_t the diameter of the atomizer nozzle or the liquid stream diameter (m), ν_m and ν_g, respectively, the kinematic viscosities of the molten metal and the gas ($m^2\,s^{-1}$) and M and G are, respectively, the mass flow rates of the metal and the gas ($kg\,s^{-1}$). G' is the gas flow rate in L/min with $G = ((G'/1000)\ \rho_g)/60$, K the experimentally determined constant for particular conditions of spray and liquid stream, in particular this constant is only available

* Corresponding author.
E-mail address: metz@univ-lyon.fr (R. Metz).

0924-0136/$ – see front matter © 2007 Elsevier B.V. All rights reserved.
doi:10.1016/j.jmatprotec.2007.01.014

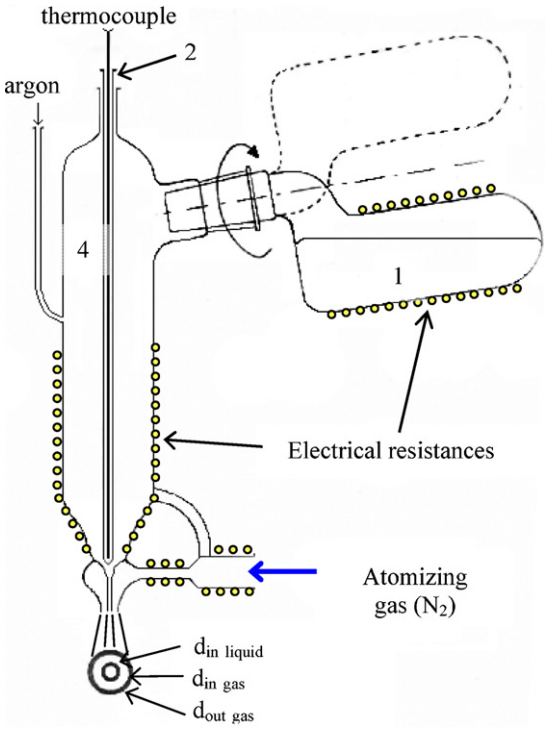

Fig. 1. Experimental molten metal atomizer.

for one pressure, W_e the dimensionless Weber's number defined as $W_e = V^2 \rho d_t/\sigma$ where the gas velocity $V = G/S\rho_g$ and ρ is the density of the metal (kg m^3), ρ_g the density of the atomizing gas (kg m^3), σ the surface tension of the liquid metal (kg s^{-2}) and S is the surface of the crown of the gas (m^2).

Two process parameters, mass flow rate and pressure of the atomizing gas, have been studied on tin metal. Indeed, few references are known on an annular configuration [15] and none with tin metal.

2. Experimental details

Tin granules of 99.9% purity were supplied by Fisher Labosi (France). The atomizing gas is nitrogen with a purity of 99.995%. The gas flowing path is illustrated in Fig. 1.

A fused silica container (item 1 in Fig. 1) is used to melt the metal. Once the metal is melted, the fused silica container is rotated (as indicated in Fig. 1) to transfer it into the atomizer proper, which is fully made in fused silica too. To reduce uncontrolled oxidation, experiments are conduced under Argon flow.

Table 1
Particle size distribution (experimental conditions: pressure of 2 bar and gas flow rate of 30 L/min)

Size (μm)	Mass (g)	Fraction	Cumulative fraction
10	0	0	0
20	0.1319	0.0033	0.0033
30	0.7973	0.0200	0.0233
40	2.3529	0.0591	0.0824
63	6.0944	0.1530	0.2354
80	4.8701	0.1223	0.3577
125	9.7853	0.2457	0.6034
250	13.0859	0.3286	0.9320
500	2.7091	0.0680	1

The fused silica container (item1) and the atomizer metal recipient (item 4) parts 1 are heated by rolled up electric resistances around the silica surface (3). The tube 2 is used to blank the nozzle so that atomization can start at the desired time. Moreover, there is a thermocouple inside the tube to indicate the temperature of the liquid metal. The atomizing gas (nitrogen) enters at the right of the system and atomizes the liquid metal by a crown of spray around the nozzle. The metal droplets are quenched into cold water or liquid nitrogen to obtain a metallic powder.

The dried atomized particles were sieved according to ASTM standard and weighted for size distribution analysis. A sample of known weight is passed through a set of sieves of known mesh sizes. They are mechanically vibrated for a period of time of 2 min. The weight of powder retained on each sieve is measured and converted into a percentage of the total powder sample.

The phases present in the powders were identified by X-ray diffractometry (XRD). The X-ray measurements were conducted in a Siemens diffractometer model using Cu Kα1 radiation with a wavelength $\lambda = 0.154$ nm. Powder XRD were determined in the $2\theta = 5$–90° range with a resolution of 0.02° and a time step of 1 s.

Characterization of the powder morphology was carried out using a Scanning Electron Microscope (SEM) Hitachi S800.

3. Results and discussion

3.1. Particle size distribution of atomized tin powders

The raw data of the particle size distribution, established by mechanical sieving, is given in Table 1. The size distribution is also depicted by the histogram and by the cumulative fraction (Fig. 2).

The statistical values calculated from the experimental data are: the median particle size (x_{med}) which is the value corresponding to 0.5 on the cumulative fraction curve, the average particle size (x_{ave}), the standard deviation (σ), the skewness

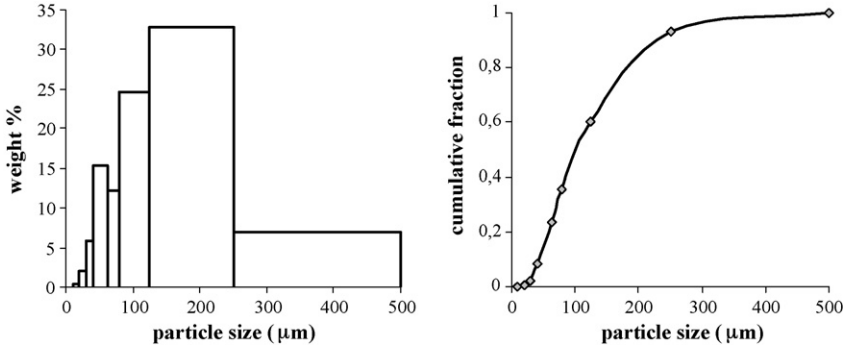

Fig. 2. Size distribution representation: histogram and cumulative fraction representations (experimental conditions: pressure of 2 bar and gas flow rate of 30 L/min).

Table 2
Statistic values for size distribution (experimental conditions: pressure of 2 bar and gas flow rate of 30 L/min)

Characteristic	Value
x_{med} (μm)	102
x_{ave} (μm)	131.5
σ	86.7
Skewness	1.3
Kurtosis	1.6

which determines the lack of symmetry around the center of the distribution and the kurtosis corresponding to a measure for peakedness.

For the same experimental conditions (pressure of 2 bar and gas flow rate of 30 L/min), these values are summarized in Table 2.

3.2. Particle size distribution modelling

The particle size distribution may be approximated by statistical functions. The most commonly used are the power law ($F(x) = 1 - (x/x_{min})^{-a}$), exponential law ($F(x) = 1 - \exp(-(x - x_{min})/x_0)$), the normal law, the log–normal law and the Rosin–Rammler law ($F(x) = 1 - \exp(-(x/x_0)^a)$) [17].

These five functions have been tested to check their suitability to the experimental size distribution.

The results summarized in Fig. 3 show that the size distribution of the atomized powders, in agreement with other studies [10,14,18], fit best the log–normal law ($R^2 > 99\%$) (the *R*-squared-values of power, exponential, Rosin–Rammler and normal law are, respectively: 0.67, 0.97, 0.93 and 0.86).

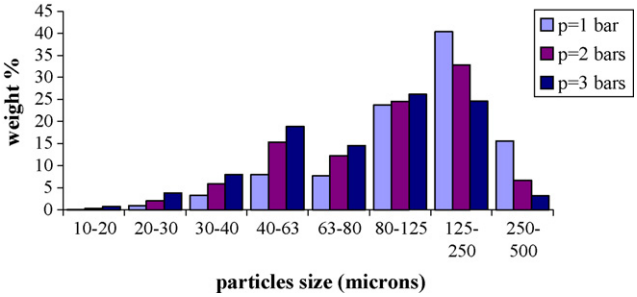

Fig. 4. Influence of the atomizing gas pressure on the size of the particles: histogram (experimental conditions: pressure of 1, 2 and 3 bar and gas flow rate of 30 L/min).

3.3. Influence of atomizing gas pressure

The influence of atomizing gas pressure on particle size distribution has been studied at three levels (1, 2 and 3 bar) with a constant gas flow rate of 30 L/min. The distribution evolution is represented by the histogram and cumulative fraction as shown in Figs. 4 and 5, respectively.

The characteristic statistical (x_{med}, x_{ave}, σ, skewness and kurtosis) values are given in Table 3. The results show that pressure variation has a strong influence on the statistical parameters of the distributions: the mass median diameter, average diameter and standard deviation decrease with increasing pressure.

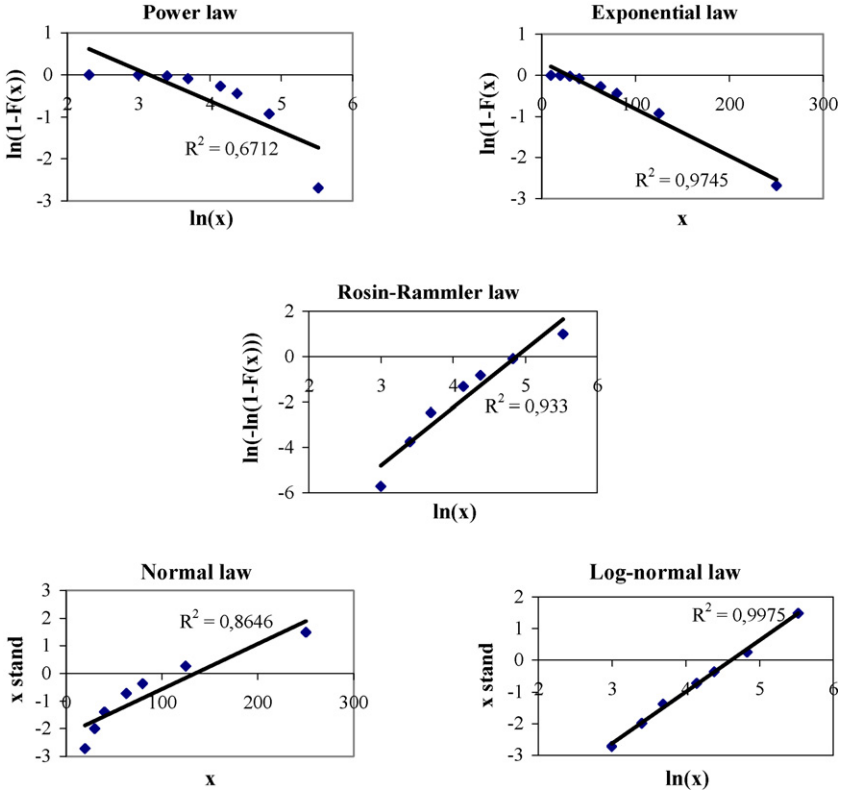

Fig. 3. Tests for approximation of particle size distribution to statistic laws (experimental conditions: pressure of 2 bar and gas flow rate of 30 L/min).

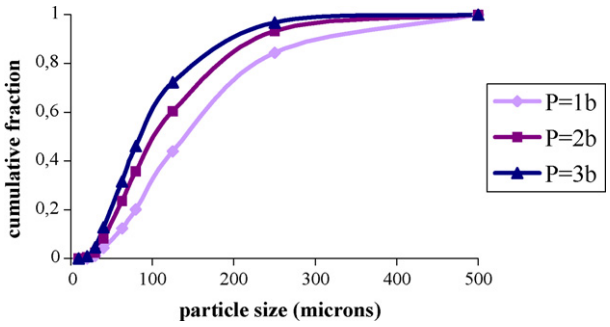

Fig. 5. Influence of the atomizing gas pressure on the size of the particles: cumulative fraction (experimental conditions: pressure of 1, 2 and 3 bar and gas flow rate of 30 L/min).

Table 3
Characteristic values for particle size distribution: influence of gas pressure (experimental conditions: pressure of 1, 2 and 3 bar and gas flow rate of 30 L/min)

P (bar)	x_{med}	x_{ave}	σ	Skewness	Kurtosis
1	140	170	102	0.9	−0.07
2	102	131	87	1.3	1.6
3	85	109	73	1.5	3.1

Other studies [11,12] confirm that increasing the pressure leads to decrease median powder particle size.

3.4. Influence of gas flow rate

Figs. 6 and 7 show the influence of the gas flow rate on the particle size distribution represented by the histogram and cumulative fraction. Table 4 summarizes the different characteristic values obtained during the present experimental work.

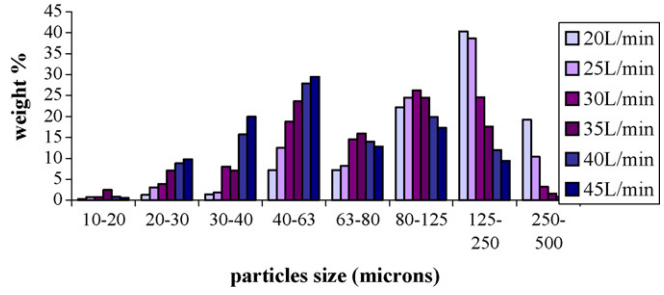

Fig. 6. Histogram for particle size distribution in function of the atomizing gas flow rate from 20 to 45 L/min ($P = 3$ bar).

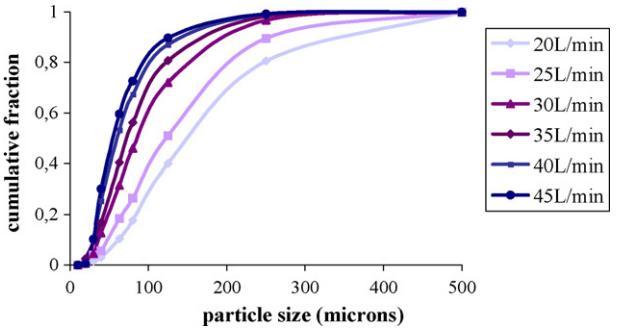

Fig. 7. Cumulative fraction for particle size distribution in function of the atomizing gas flow rate from 20 to 45 L/min ($P = 3$ bar).

Table 4
Characteristic values for particle size distribution: influence of gas flow rate (experimental conditions: pressure of 3 bar and gas flow rate from 20 to 45 L/min)

Flow rate (L/min)	x_{med}	x_{ave}	σ	Skewness	Kurtosis
20	149	181	107	0.7	−0.5
25	123	150	95	1.1	0.7
30	85	109	73	1.5	3.1
35	72	92	63	1.7	4.2
40	60	78	55	2	5.9
45	55	72	52	2.3	7.6

Consistent with other studies [14,18], the present results demonstrate that the mass median diameter x_{med} decreases when increasing the atomizing gas flow rate. The average diameter x_{ave} shows similar behaviour. The spread of the size, represented by the standard deviation, σ, increases also for low atomizing gas flow rates indicating that relatively a higher proportion of large particles are present in such powders.

3.5. Correlation between the Lubanska equation and experimental data

Table 5 compares the experimental data with the calculated values for different gas flow rates and gas pressures. The experimental and calculated mean diameters are in good agreement. This formula can then estimate the particle mean diameter for different values of gas flow rates and pressures.

It is now interesting to verify if this mathematical function confirms the experimentally determined influence of these two parameters on the mean diameter of the powder particles. The Lubanska formula suggests that the mean particle diameter decreases with increasing the atomizing gas flow rate: $d_m = d_t K[(\nu_m/\nu_g)(S^2\sigma\rho_g^2/G^2\rho d_t)(1 + M/G)]^{1/2}$. It confirms the experimental data given in Figs. 4 and 5 and in Table 2.

3.6. Study of particle morphology

The influence of the quenching liquid (cold water or liquid nitrogen) on the form of the metallic particles has been studied.

Table 5
Comparison between the experimental (d_{exp}) and calculated (d_{cal}) mean diameters

Flow rate (L/min)	$P = 1$ bar		$P = 2$ bar		$P = 3$ bar	
	d_{exp} (μm)	d_{cal} (μm)	d_{exp} (μm)	d_{cal} (μm)	d_{exp} (μm)	d_{cal} (μm)
20	200	206	168	158	149	143
25	174	159	148	128	123	106
30	140	139	102	99	85	85
35	–	–	87	86	72	71
40	–	–	–	–	60	61
45	–	–	–	–	55	54

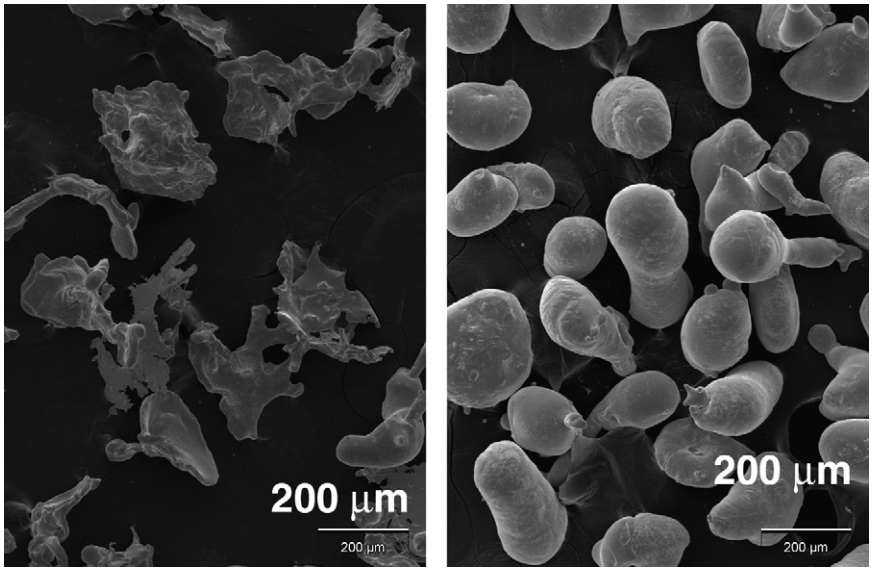

Fig. 8. Influence of the liquid quench on the morphology of the particles (125–250 μm): at the top, particles quenched into cold water and at the bottom, particles quenched into liquid nitrogen.

The SEM photographs show that particles quenched in liquid nitrogen have a more spherical or oblong shape and are smoother (Fig. 8). Moreover, it will be seen on the next SEM photograph that the sphericity of the particles increase with the decrease of the size distribution range of the powder and that the powder shape is more spherical and regular (Fig. 9). These observations may be interpreted on the basis of the difference between the specific heat capacity and thermal conductivity between water and nitrogen which are $0.61\,W\,m^{-1}\,K^{-1}$ versus $0.13\,W\,m^{-1}\,K^{-1}$ and $4.18\,J\,g^{-1}\,K^{-1}$ versus $2.04\,J\,g^{-1}\,K^{-1}$, respectively. A drop of metal falling into liquid nitrogen should cool slower than in a water medium. Moreover, the spherical shape may find its origin by the creation of a film of nitrogen gas wrapping the drops of liquid metal during the quench operation.

A polished cross-section of these metal particles has been examined to assess the powder internal densification. The powder particles were mounted into a polymeric resin and the resin was polished until the particles are cut around the middle. An example of a SEM image is shown in Fig. 10. The surface of this cross-section presents some scratches due to burnishing. It can

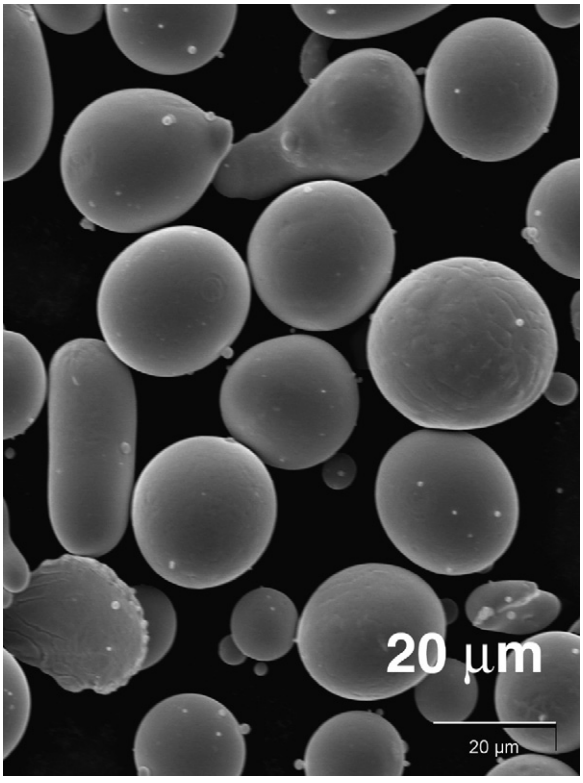

Fig. 9. Influence of the liquid quench on the morphology of the particles (20–30 μm): at the top, particles quenched into cold water and at the bottom, particles quenched into liquid nitrogen.

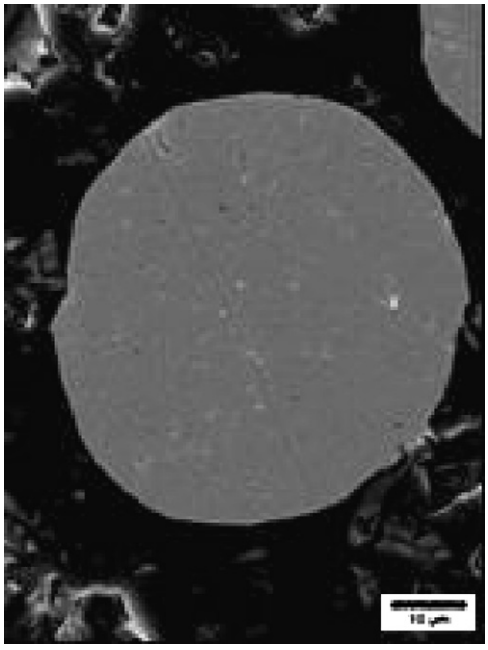

Fig. 10. SEM photo of a cross-section of a particle of tin (40–63 μm).

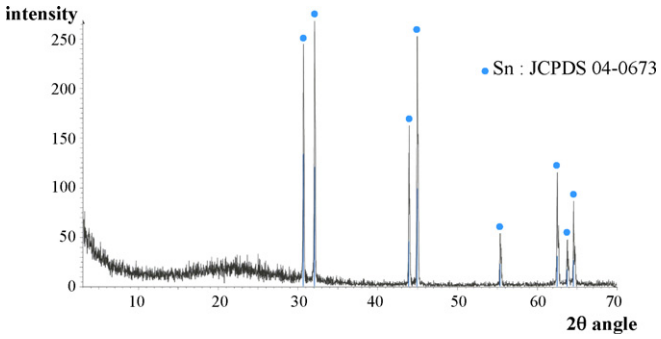

Fig. 11. X-ray diffraction diagram of an atomized tin powder.

be noted that the particle is fully densified and does not present any apparent macroscopic porosity.

3.7. Analysis of the purity of the obtained powders

X-ray diffraction analysis has been carried out to check the absence of foreign phases. Pollution could indeed arise from the interaction between the molten metal and the atomizing gas or the quenching media (cold water or liquid nitrogen) inducing the formation of nitrides or oxides.

Fig. 11 shows a typical PXRD pattern. In the limiting detection of 2% of the X-ray, it was not possible to detect any by-product as a consequence of a reaction between molten tin and its surrounding.

4. Summary

This study gives a full characterization of atomized tin. Particle size distribution with histogram and cumulative fraction representations, with location, width, asymmetry and peakedness descriptors, and the approximation of the distribution by the log–normal function and with the phase and morphology have been determined.

These atomization experiments confirm the strong influence of two processing variables (gas pressure and gas flow rate) on particle size distribution. It has been shown that increasing gas flow rate or gas pressure leads to a decrease of median particle size and width of the distribution measured by standard deviation.

The experimental size distributions have been successfully approximated by a log–normal law after comparison with other commonly used mathematical functions.

In the experimental range study, the Lubanska formula has been successfully applied to tin metal powders obtained by atomization through an annular nozzle.

Moreover, the influence of the quenching liquid on the particle morphology has been demonstrated and liquid nitrogen seems to be the preferable choice to make spherical particles.

Moreover, powders obtained by atomization do not show any pollution due to this process.

References

[1] H.A. Kuhn, A. Lawley, Powder Metallurgy Processing. New Techniques and Analyses, Academic Press, 1978.
[2] R. Metz, H. Delalu, J.R. Vignalou, N. Achard, M. Elkhatib, Electrical properties of varistors in relation to their true bismuth composition after sintering, Mater. Chem. Phys. 63 (2000) 157–162.
[3] R. Metz, C. Machado, M. Hassanzadeh, R. Puyané, Direct oxidation of an alloy precursor. Complete oxidation of bismuth and zinc powder, J. Electroceram. 13 (2004) 825–827.
[4] S. Lagutkin, L. Achelis, S. Sheikhaliev, V. Uhlenwinkel, V. Srivastava, Atomization process for metal powder, Mater. Sci. Eng. A 383 (1) (2004) 1–6.
[5] S. Özbilen, Studies of gas atomization of aluminium, copper, zinc, tin and aluminium alloy powders, Met. Powder Rep. 55 (6) (2000) 36.
[6] I.P. Goldaev, A.P. Motornenko, A.P. Shevchenko, Yu.A. Lastivnyak, Gas-jet atomization of liquid metals and alloys, Poroshkovaya Metallurgiya (Kiev) 11 (2) (1971) 9–13.
[7] P. Gummeson, P. Ulf, Modern atomizing techniques, Powder Metall. 15 (29) (1972) 67–94.
[8] K.P. Rao, S.P. Mehrotra, Effect of process variables on atomization of metals and alloys, Mod. Dev. Powder Metall. 12 (1981) 113–130.
[9] U.R. Date, U.R. Tendolkar, S. Gangadar, M.N. Vartak, Statistical interpretation of metal atomization, Int. J. Powder Metall. (New York) 3 (2) (1967) 49–55.
[10] A. Ünal, Effect of processing variables on particle size in gas atomization of rapidly solidified aluminium powders, Mater. Sci. Technol. 3 (1987) 1029–1039.
[11] G. Helmersson, A. Hede, T. Johannesson, B. Bergman, H. Hallen, On the control of powder-size distribution in full-scale gas atomization of nickel-based alloys, Scand. J. Metall. 26 (1997) 93–101.
[12] K. Tamura, T. Takeda, A study on production pf copper powder by atomization, Trans. Natl. Res. Inst. Met. 5 (1963) 252–256.
[13] J.K. Beddow, Powder Monographs in Science and Technology. The Production of Metal Powders by Atomization, A.S. Goldberg, 1977.
[14] K.Y. Kim, W.R. Marshall, Drop-size distributions from pneumatic atomizers, AIChE J. 17 (1971) 575–584.
[15] H. Lubanska, Correlation of spray ring data for gas atomization of liquid metals, J. Met. 22 (2) (1970) 45–49.
[16] L.D. Wigg, Drop-size prediction for twin-fluid atomisers, J. Inst. Fuel 11 (1964) 46–52.
[17] P.J.T. Verheijen, Statistical Distributions in Particle Technology, Particle Technology Course, Department of Chemical Engineering, Technical University Delft, The Netherlands, 2001.
[18] J. Juarez-Islas, Y. Zhou, E.J. Lavernia, Spray atomization of two Al–Fe binary alloys: solidification and microstructure characterization, J. Mater. Sci. 34 (1999) 1211–1218.